ISBN: 978-3-95450-221-9 ISSN: 2226-0358 doi:10.18429/JACoW-ICALEPCS2021-WEPV002

POSITION SCANNING SOLUTIONS AT THE TARUMÃ STATION AT THE CARNAÚBA BEAMLINE AT SIRIUS/LNLS

C. S. N. C. Bueno†, L. G. Capovilla, R. R. Geraldes, L. C. Guedes, G. N. Kontogiorgos, L. Martins dos Santos, M. A. L. Moraes, G. B. Z. L. Moreno, A. C. Piccino Neto, J. R. Piton, H. Tolentino, Brazilian Synchrotron Light Laboratory (LNLS), CNPEM, Campinas, Sao Paulo, Brazil.

Abstract

TARUMÃ is the sub-microprobe station of the CARNAÚBA beamline at Sirius/LNLS. Covering the range from 2.05 to 15keV, the probe consists of a fully-coherent monochromatic beam varying from 550 to 120nm with flux of up to 1e11ph/s/100mA after the achromatic focusing optics. Hence, positioning requirements span from nanometer-level errors for high-resolution experiments to fast continuous trajectories for high throughput, whereas a large flexibility is required for different sample setups and simultaneous multi-technique X-ray analyses, including tomography. To achieve this, the overall architecture of the station relies on a pragmatic sample position-ing solution, with a rotation stage with a range of 220°, coarse stages for sub-micrometer resolution in a range of 20mm in XYZ, and a fine piezo stage for nanometer resolution in a range of 0.3mm in XYZ. Typical scans consist of continuous raster 2D trajectories perpendicularly to the beam, over ranges that vary from tens to hundreds of micrometers, with acquisition times in range of milliseconds. Positioning based on 4th-order trajectories and feedforward, triggering including the multiple detectors and data storage are addressed.

INTRODUCTION

TARUMÃ [1] is the sub-microprobe station of the CARNAÚBA beamline [2] at Sirius/LNLS [3]. The CARNAÚBA beamline was designed to cover the range from 2.05 to 15keV, and is based on an all-achromatic optical design. The probe consists of a fully-coherent monochromatic beam varying from 550 to 120nm, focused by a set of KB (Kirkpatrick-Baez) mirrors, and with flux of up to 1e11ph/s/100mA. TARUMÃ was designed to perform simultaneous multi-technique analyses under a variety of conditions, including *in situ*, *in vivo*, and *in operando* experiments. Thus, it complies a number of customized sample environments [1, 4, 5] and a set of detectors of different types, including: two SDD Vortexes (Xspress 3 and Xspress 3X), two area detectors (MobiPix 45D and PiMega 135D, one XEOL detector, and an in-house spectrometer. Figure 1 shows a detailed view of the sample and the detectors (left) and an overview picture of the TARUMÃ station (right).

The sample stage is composed, from bottom up, of: an Aerotech's 300DL XY, a Newport's IDL280 Z20 wedge-type vertical stage, an Aerotech's ABRS 250MP air-bearing rotary stage, and a PI's P-563.3 XYZ stage. The planar and vertical stages are responsible for the rough alignment of the sample with a range of ±10mm in XYZ. The rotary stage, constrained over 220° due to cable management, is used for tomography, diffraction, and Bragg CDI experiments. A cable carrier system allows additional instrumentation, like special gases, heaters, sensors, and vacuum lines, to be used in the sample environment. The XYZ piezo stage is responsible for the sample scans with nanometer resolution over a 300µm range and has a payload capacity of 5 kg.

Resolutions down to the order of 10nm are desired from the experiment's reconstructions, which sets an upper boundary for the relative positioning errors between the sample and the KB mirrors. Thus, to reach these positioning levels, the KB optics and the sample stage are placed

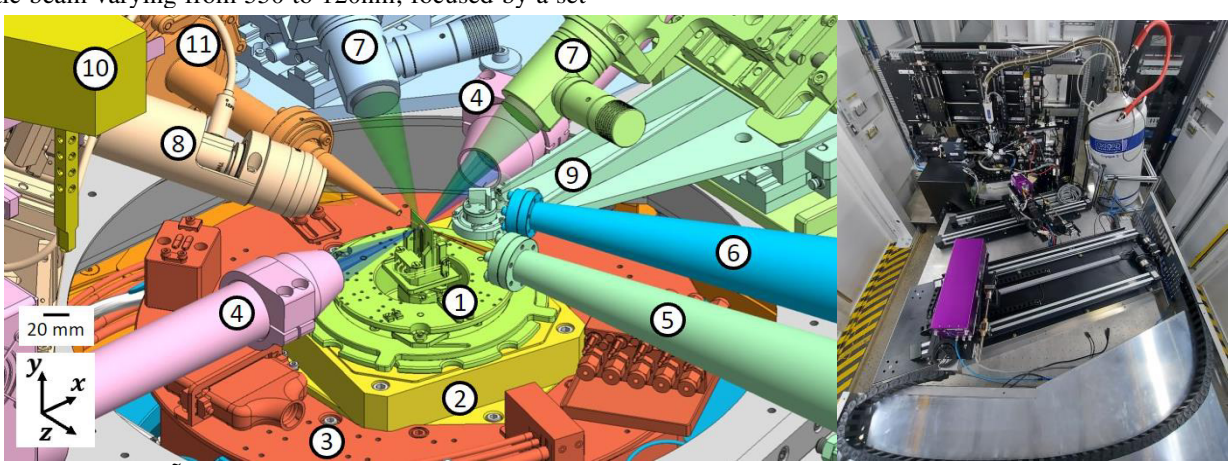

Figure 1: TARUMÃ station: drawing of the region surrounding the sample, detailing: the sample setup(1), the sample stage (2 and 3), the fluorescence detectors (4), the flying paths for the transmission(5) and the diffraction(6)area detectors, the optical microscopes (7), the XEOL optics (8), a crystal analyser spectrometer (9), the pick-and-place gripper (10), and the KB vessel exit port (11). (left) and assembly status on 10/07/2021 (right).

† cassiano.bueno@lnls.br

ISBN: 978-3-95450-221-9 ISSN: 2226-0358 doi:10.18429/JACoW-ICALEPCS2021-WEPV002

above a common granite bench [1]. Furthermore, to have a more accurate estimate of the sample position with respect to the focusing optics, a metrology target on the rotor of the rotary stage is measured by 3 capacitive sensors on an external metroframe fixed to the granite bench. Hence, the information of the capacitive metrology can be combined with the data from P-563.3 capacitive sensors to improve the post-processing reconstructions. Finally, the controller of each stage is designed and optimized for the system to achieve the required nanometric resolution.

More information on the overall dynamic design and the other subsystems can be found in [1]. This paper describes the main implementation aspects of the sample positioning system and the related control required for this state-of-the-art X-ray microscopy station. First, the integrated control architecture is reviewed. Next, the high-performance motion control and trajectories are discussed. Finally, commissioning results are presented to demonstrate the current capabilities.

INTEGRATION ARCHITECTURE

Being TARUMÃ a multi-technique end-station that aims at nanometric resolution and high throughput, it requires, besides the dynamic and motion optimization, a high degree of integration between detectors and motion system, as well as a robust system that can perform hundreds of experiments on a daily basis. Past solutions at the 2nd-generation UVX light source at LNLS generally relied on EPICS (Experimental Physics and Industrial Control System) variables to control sample motion and detectors acquisition. Back then, the default update rates up to 10Hz did introduce overhead time in measurements, but those were acceptable due to the lower fluxes available to the beamlines, with correspondingly longer total experiment times. At SIRIUS 4th-generation machine, on the other hand, with photon fluxes up to 1000 fold, the experiment times can be drastically shortened and different types of experiments are required, such that previous solutions become incompatible with TARUMÃ's purposes and capabilities. Therefore, a new solution was proposed and implemented, in which all motion systems and detectors are interconnected via TTL signals that enable fast communication and synchronization among systems, allowing experiments to be up to 130 times faster.

Figure 2 summarizes the integration architecture implemented at TARUMÃ, with the control and detection hardware, and the corresponding signal connections. It is based on the Trigger And Timer Unit (TATU) solution, a flexible in-house development for FPGA-based applications created on NI's CompactRIO (cRIO) [6]. Indeed, capable of receiving leading signals and distributing them to the elements in the control network, such as motion controllers and detectors, it also allows for simple logic operations, customized delays and pulse counting of TTL signals, which can be used for synchronizing motion and data acquisition. Any motion controller with a digital output and capable of reading a trajectory file is suitable as the leading system, depending on the scan routine to be executed. This versatility is what makes the solution easily expandable and general enough to be applied to different beamlines.

At TARUMÃ, the core and most demanding task consists in high-resolution 2D mapping with the XYZ piezo stage. Thus, the standard operation is based on a Main cRIO with an in-house FPGA code that: 1) reads a trajectory file at a 10 kHz rate; 2) translates it into proportional voltage signals that are sent to the XYZ motion controller PI E-727; and 3) provides trigger signals to TATU, running in an independent cRIO,. Hence, TATU's output signals

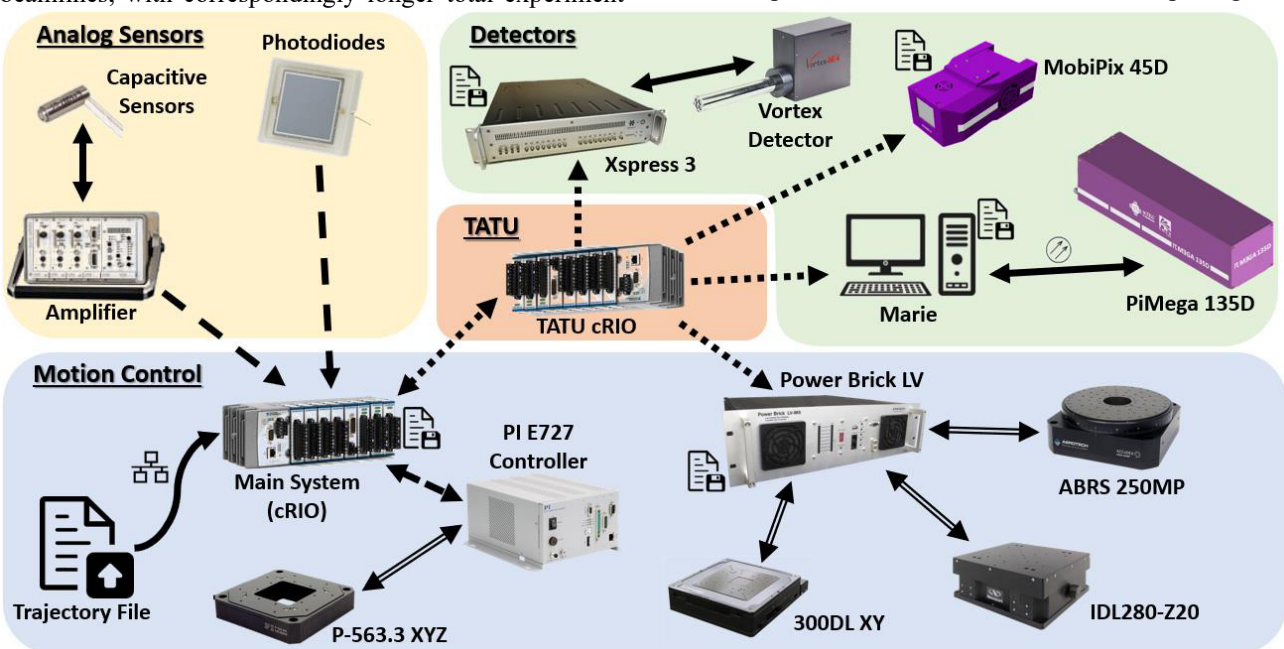

Figure 2: Integration architecture at the TARUMÃ station. The different arrows represent different signal types, namely: solid lines (-) are data transfer signals, dashed lines (--) represent analog signals, dotted lines (.) represent trigger signals and the double thin lines (=) represent closed-loop control signals (feedback and actuators).

ISBN: 978-3-95450-221-9 ISSN: 2226-0358 doi:10.18429/JACoW-ICALEPCS2021-WEPV002

can be used to trigger and synchronize acquisition for: 1) the detectors, with images and energy spectra; 2) the analog signals, which include photodiodes, the capacitive sensors on the metrology frame, and the capacitive sensors in PI P-563.3 stage; and 3) the encoder data from the Omron Delta Tau Power Brick LV (PBLV) sample stage controller, which is further used in 2D and 3D reconstructions.

Nowadays, following a common practice regarding software operation at Sirius beamlines, the fly-scans are planned on a Jupyter Notebook [7], hosted in a Jupyter server that runs on the beamline operation computer. The script is written in Python and allows the user to select: the detectors, the energy regions of interest (ROI) for fluorescence, and the desired trajectory to performed. Currently, 25 predefined trajectories are directly available, as detailed in the following section, whereas unforeseen trajectories may accepted but must be previously calculated and deployed to the cRIO memory. In the near future, the Jupyter Notebook functionality is expected to be expanded with a friendly graphical interface, according to already existing Sirius standards and software tools, in which new trajectories will be dynamically calculated from user input parameters. The Jupyter Notebook is also programmed to configure all detectors and EPICS IOCs desired parameters, such as the number of points and the filenames to be saved.

A fly-scan data-flow example is summarized in Fig. 3. After setting all parameters, the selected trajectory starts with the Main cRIO moving the XYZ piezo stage and sending the trigger signal to TATU, which is properly broadcast to the detectors and complementary controllers. By the end of the task, the files created in each sub-system are merged into one final experiment file and saved in a central storage. Due to the large amount of data generated by the detectors, the files are merged in a powerful Power 8 desktop computer, known by its nickname “Marie”, and then sent to the data storage.

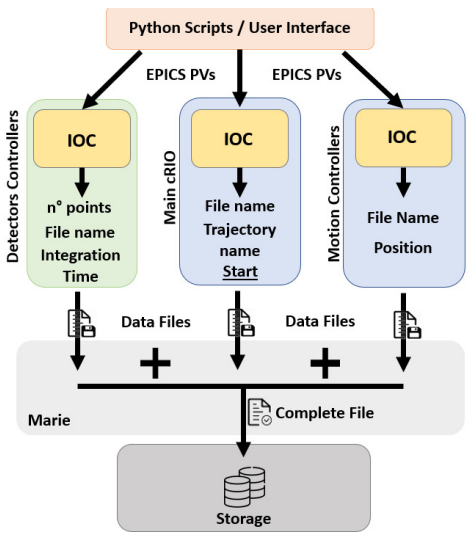

Figure 3: Data-flow schematic in TARUMÃ fly-scans, from the user interface to the data storage.

Still, the flexibility and the easiness in programing the Jupyter Notebook routines in the implemented solution make it possible to include these fly-scans in broader tasks with other beamline components, such as: the sample rotary stage, for tomography; the four-crystal monochromator, for spectroscopy; and the coarse XZ and Y sample stages to perform long-range high-resolution images via stitching. All these different processes have already been successfully commissioned at TARUMÃ, but are also continuously updated and expanded.

MOTION CONTROL

Models and Guidelines

To reach the nanometric positioning capacity, mechanical and control and aspects of the entire station must be taken in count. To help the studies regarding trajectories simple lumped-mass models, as exemplified in figure 4, were implemented to simulate vertical and lateral performances of sample stage and guide motion strategies. The mechanical stiffness between stages and inside the stages (rotor-to-stator) were measured or estimated. In addition, to more accurately derive the models, the individual closed-loop responses were either measured, for the Aerotech DL300 XY and PI 563.3 stages, or estimated, for the IDL280 Y stage, and individually matched in the separate models, before finally integrated.

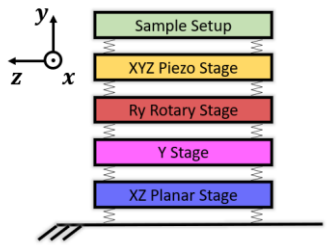

Figure 4: Lumped mass model of the sample stack, used to evaluate vertical and lateral positioning performances.

Firstly, to instruct towards the most suitable trajectory orientation, Fig. 5 depicts the simulated closed-loop Bode plot, both for the vertical and horizontal axes, from the commanded position reference in the P-563.3 to the absolute position of the sample in an arbitrary sample holder weighing 300 g. It can be seen that the vertical axis has a higher bandwidth, around 60Hz, as compared to the horizontal axis, around 20Hz. Thus, the vertical axis exhibits a higher virtual stiffness against disturbances, and can also follow more aggressive trajectory setpoints (velocities and accelerations).

Next, the models were used to investigate the impact of the trajectories on the sample stack, due to, for example, the reaction forces induced in the stages below, with corresponding control errors. Two types of *S-curve* trajectories were considered, namely: 3rd [8] and 4th [9] orders. Third order trajectories are simpler and more commonly employed in commercial motion controllers, but since fourth order trajectories are smoother, due to the higher order continuous derivates, this application was taken as a case study to compare both solutions.

ISBN: 978-3-95450-221-9 ISSN: 2226-0358 doi:10.18429/JACoW-ICALEPCS2021-WEPV002

Figure 6 displays the simulated disturbances induced by trajectories of 14.5µm, with 20µm/s cruise velocity, maximum acceleration of 100µm/s^2 and maximum jerk of 1000µm/s^3. The difference lies in the 4th order limiting also the jerk derivate (snap) in 2400µm/s^4. The simulations are for the more compliant horizontal axis for the sake of demonstration, reaching errors in the order of a few nm, but equivalent results in the sub-nm range (scaled roughly by a factor 10) would were found for the vertical axis. Naturally, the magnitude of these errors vary for different accelerations and payloads, but it is possible to notice that the total disturbances induced in the planar stage can be significantly lower and smoother with a 4th-order trajectory, as expected.

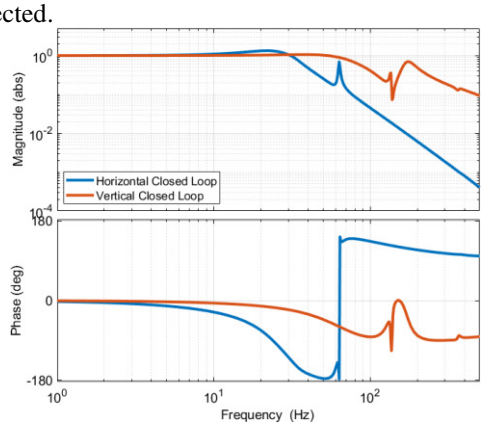

Figure 5: Closed-loop Bode plot for the sample stack in the vertical and horizontal axes, from the P-563 stage reference to the absolute sample position.

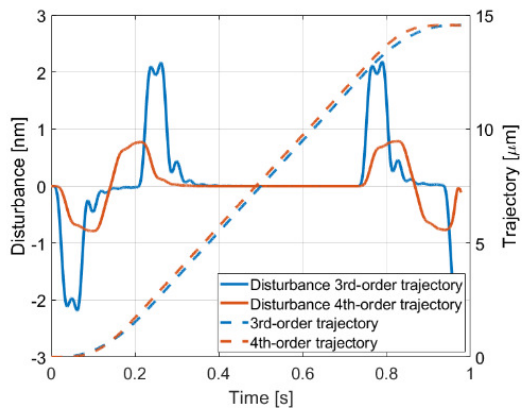

Figure 6: Simulated induced disturbances in the planar 300DL for 3rd and 4th-order trajectories with the P-563.

Trajectories

Based on the previous observations, 4th-order trajectories with the most aggressive setpoints in the vertical axis were chosen for the beamline operation. Then, to cover 2D maps, the fly-scan profile that has been used so far at TARUMÃ is shown in Fig. 7, being composed of long vertical and short horizontal 4th-order trajectories that are concatenated to form a snake-raster pattern. The scans are defined by the following user inputs: vertical velocity, the vertical and horizontal stroke, the trigger length per acquisition point, and the horizontal pitch.

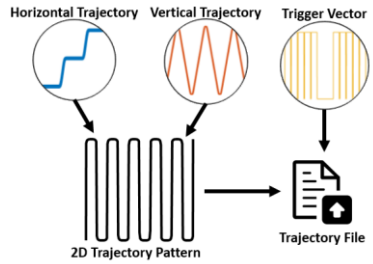

Figure 7: 2D fly-scan pattern at TARUMÃ, highlighting the horizontal and vertical 4th-order trajectories, and the trigger vector as a function of time

To simplify the post-processing of data, the vertical trajectory is calculated so that the constant velocity segment has the exact length of the desired scanning ROI selected by the user. The horizontal trajectory starts when the vertical trajectory is deaccelerating, and it is optimized so that to the horizontal motion ends just before the start of the next constant velocity segment in the vertical axis. This ensures that the accelerations and, consequently, the forces that are applied due to the horizontal motion in the stages below are minimized during acquisition.

The scan vectors are described in 10kHz, which is five to ten times faster than the maximum acquisition rates of 1 to 2kHz that are planned for the beamline. They are saved in the file to be consumed during the experiments. Moreover, besides the vertical and horizontal trajectories, a trigger vector is included in the same file, consisting of a pulse train in which the high level designates acquisition to detectors, such that the acquisition time for each point (integration time) is defined by the pulse width.

Performance refinement

The first offline tests with the piezo XYZ stage indicated following error peaks of up to 500nm for the desired 4th-order vertical trajectories, which might critically compromise data post-processing or at least burden it by requiring more iterations before the final image reconstruction. In that way, the position feedforward gain (*kff*) available in the E-727 controller was studied to optimize the following errors. Figure 8 shows the P-563 stage control error for different scenarios, emphasizing the importance of including an optimal feedforward gain, with improvements by up to a factor 5.

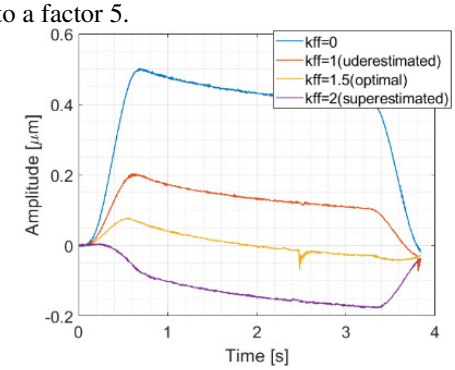

Figure 8: Following errors measured with the P-563 stage for a 4th-order vertical trajectory with different position feedforward gains in E-727 controller.

ISBN: 978-3-95450-221-9 ISSN: 2226-0358 doi:10.18429/JACoW-ICALEPCS2021-WEPV002

Another concern regarding the system controller is the diversity of sample holders that will be used at TARUMÃ, with different weights, and various boundary conditions like gases, vacuum, and temperature. Indeed, keeping control errors and trajectory following performances in the desired levels becomes a practical challenge. The current solution is to previously characterize and optimize the control parameters, including the feedforward gain, for each different setup and provide a selectable controller to the beamline user. For future experiments, a new routine will be developed to automatically optimize (as much as possible) the control parameters for each sample in each sample holder. Such solutions are only possible thanks to the integration of the E-727 controller in EPICS, that allows to easily update the control parameters.

RESULTS

Using the discussed implementation, the first commissioning tests at the beamline, still without beam, were performed during the storage ring 2020/2021 holidays shutdown, whereas the first tests with beam took place in early March 2021. The implementation of the fly-scan routine made it possible to significantly increase the number of experiments performed daily at the CARNAÚBA beamline. For comparison, a 10x10µm^2 mapping, with 10.000 points (100nm resolution) using the previous EPICS-based architecture would take a total of about 2.8 hours, i.e. almost 1s per point. Using the new fly-scan architecture, on the other hand, the same experiment required just 250s before some control optimization and only 75s after that, resulting in a gain of 130 fold for the same quality. Figure 9 shows a florescence image (left) and the ptychography reconstruction (right) of an USAF pattern that is used for beam characterization, validating the motion control and the synchronization between different detectors (for more details, see [2]). The image was acquired in 130s, with a 5x5µm^2 scan and 6.25ms integration time per point.

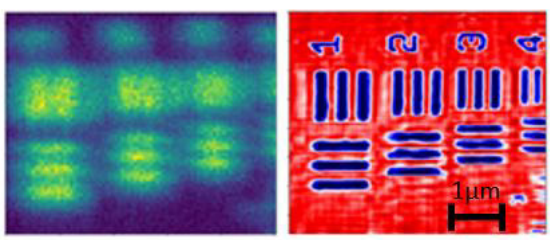

Figure 9: USAF pattern in fluorescence (left) and ptychography (right), with resolution of 300 nm (out of focus) and 70 nm, respectively, validating the synchronism between detectors and motions system.

In addition to throughput, the improvement in experiment time helps minimizing the effects of experimental disturbances, such as vacuum and temperature interlocks, that in the past have been responsible for acquisition losses with the previous architecture. This gain also accelerated several steps in the beamline commissioning, as refinement in mirrors alignment, correction of the KB astigmatism, and commissioning of detectors. Moreover, the minor time per experiment and the modular characteristic of the implementation made it possible to step forward to more advanced experimental routines like energy scans (spectroscopy), tomography, and large 2D mapping (up to 2mm) with sub-micron resolution.

Due to ongoing commissioning and studies regarding the area detectors, the integration time in ptychography and florescence is currently limited to a minimum of 5ms per point, with velocities around 50µm/s to avoid data loss. During aligment, in turn, especial trajectories with 500µs of integration time can be used with transmission data in photodiodes, since the cRIO that acquires the analog signals is capable of measurements up to 100kHz. Yet, to reach sub-ms integration time, velocity must be increased up to 800µm/s, leading to large following errors in addition to making it necessary to rearrange and interpolate the detectors data with respect to the encoders data to compose the final images. Nevertheless, even with interpolation, the quality loss is sufficient for aligment purposes.

As an example, Fig. 10 shows 80x80µm^2 absorption images of a sample with 800nm pixel size, with mapping both in fast scanning with 500µs of integration time (total time of 30s including overhead) in the left, and in standard scanning with integration time of 10ms (total time of 140s including overhead).

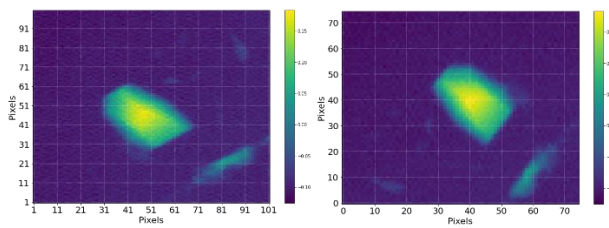

Figure 10: Sample absorption images for interpolated fast mapping at 800µm/s (left) and standard 40µm/s (right).

CONCLUSION

The successful deployment of the first version of fly-scan mapping at TARUMÃ is questions and challenges to a next level. The 100-fold faster scan solution allows the scientists and beamline staff to have immediate answers for samples and the commissioning equipment. Moreover, the general and flexible control architecture enables other motion systems, like the sample coarse stages, or the monochromator, to be integrated to the detectors and perform fast scans as well. The next challenges include the creation of a friendly user interface, and the design of an automatic routine to optimize control parameters for different samples and sample environments. Concerning of more complex experiments, tomography alignment and execution routines and Power Brick fly-scans are under development.

ACKNOWLEDGEMENTS

The authors would like to gratefully acknowledge the funding by the Brazilian Ministry of Science, Technology and Innovation, and the contribution and diligent work of the LNLS teams.

ISBN: 978-3-95450-221-9 ISSN: 2226-0358 doi:10.18429/JACoW-ICALEPCS2021-WEPV002

REFERENCES

[1] R. Geraldes et al., "Design and Commissioning of the TARUMÃ Station at the CARNAÚBA Beamline at Sirius/LNLS", presented at. MEDSI 2020, Chicago, USA, Jul. 2021, paper WEPB13, unpublished.

[2] Tolentino, H.C.N., et al., "X-ray microscopy developments at Sirius-LNLS: first commissioning experiments at the Carnauba beamline", in *Proc*. SPIE X-Ray Nanoimaging: Instruments and Methods , San Diego, California, USA, Sep. 2021, doi: 10.1117/122596496.

[3] Sirius Project, https://www.lnls.cnpem.br/sirius-en/.

[4] W. H. Wilendorf et al., "Electrochemistry and Microfluidic for the TARUMÃ Station at the CARNAÚBA Beamline at Sirius/LNLS", presented at. MEDSI 2020, Chicago, USA, Jul. 2021, paper WEPC03, unpublished.

[5] F. R. Lena et al., "A Cryogenic Sample Environment for the TARUMÃ Station at the CARNAÚBA Beamline at Sirius/LNLS", presented at. MEDSI 2020, Chicago, USA, Jul. 2021, paper WEPC02, unpublished.

[6] J. R. Piton et al, "TATU: a flexible FPGA-based trigger and timer unit created on CompactRIO for the first SIRIUS beamlines", presented at the 18th Int. Conf. on Accelerator and Large Experimental Physics Control Systems (ICALEPCS'21), Beijing, China, Oct 2021, paper THPV021, this conference.

[7] Jupyter Notebook, https://jupyter.org/.

[8] P. Lambrechts, "Trajectory planning and feedforward design for electromechanical motion systems", TUE, Eindhoven, Netherlands Rep. DTC 2003-18, Apr. 2003.

[9] Advanced Setpoints for Motion Systems, https://www.mathworks.com/matlabcentral/fileexchange/16352-advanced-setpoints-for-motion-systems